

# Premature thymic involution is independent of structural plasticity of the thymic stroma

Dean Franckaert<sup>\*1,2</sup>, Susan M. Schlenner<sup>\*1,2</sup>, Nathalie Heirman<sup>1,2</sup>,  
Jason Gill<sup>3</sup>, Gabriel Skogberg<sup>4</sup>, Olov Ekwall<sup>4</sup>, Karen Put<sup>1,2</sup>,  
Michelle A. Linterman<sup>5</sup>, James Dooley<sup>\*\*1,2</sup> and Adrian Liston<sup>\*\*1</sup>

<sup>1</sup> Autoimmune Genetics Laboratory, VIB, Leuven, Belgium

<sup>2</sup> Department of Microbiology and Immunology, University of Leuven, Leuven, Belgium

<sup>3</sup> Mechanisms of Cancer, Friedrich Miescher Institute for Biomedical Research, Basel, Switzerland

<sup>4</sup> Department of Rheumatology and Inflammation Research, Göteborg University, Gothenburg, Sweden

<sup>5</sup> Lymphocyte Signaling and Development ISP, Babraham Institute, Cambridge, UK

The thymus is the organ devoted to T-cell production. The thymus undergoes multiple rounds of atrophy and redevelopment before degenerating with age in a process known as involution. This process is poorly understood, despite the influence the phenomenon has on peripheral T-cell numbers. Here we have investigated the FVB/N mouse strain, which displays premature thymic involution. We find multiple architectural and cellular features that precede thymic involution, including disruption of the epithelial–endothelial relationship and a progressive loss of pro-T cells. The architectural features, reminiscent of the human thymus, are intrinsic to the nonhematopoietic compartment and are neither necessary nor sufficient for thymic involution. By contrast, the loss of pro-T cells is intrinsic to the hematopoietic compartment, and is sufficient to drive premature involution. These results identify pro-T-cell loss as the main driver of premature thymic involution, and highlight the plasticity of the thymic stroma, capable of maintaining function across diverse interstrain architectures.

**Keywords:** FVB/N mouse · Involution · Pro-T cells · Thymic epithelium cells · Thymus · Vascularization



Additional supporting information may be found in the online version of this article at the publisher's web-site

## Introduction

The thymus is responsible for the differentiation and maturation of T cells from BM precursors. The stromal cells in the thymic microenvironment – a population that includes cortical thymic epithelial cells (cTEC), medullary thymic epithelial cells (mTEC),

fibroblasts, and endothelium – provide the microenvironmental instructions for T-cell differentiation [1, 2]. With the physiological necessity of the thymus for the differentiation of BM stem cells into mature T cells, the migration of progenitor cells into the thymus is a key event. Until recently, the early thymic progenitors, known as pro-T cells, were thought to have limited self-renewing capacity,

**Correspondence:** Dr. Adrian Liston  
e-mail: adrian.liston@vib.be

\*These authors contributed equally to this work as first authors.

\*\*These authors contributed equally to this work as last authors.

forcing the thymus to rely on the periodic release of progenitors from the BM for continued T-cell differentiation [3–6]. More recent experiments demonstrate that progenitor cells do indeed possess indefinite self-renewal capacity, with the population turnover driven by forced displacement by new pro-T cells [7]. This immigration of precursors relies on chemokines such as CCL25 and adhesion molecules (P-selectin, alpha 6 integrin, VCAM-1, ICAM-1) presented by endothelium of the postcapillary venules at the cortical–medullary junction [5, 8, 9]. Following entry into the thymus, the differentiation of these BM-derived precursors requires extensive crosstalk between the multiple cellular components of the thymus, all of which are necessary for the processes of proliferation; differentiation; T-cell receptor (TCR) rearrangement; positive and negative selection; and finally lineage commitment, maturation, and emigration [10].

Unique among organs, the thymus undergoes a series of seemingly well-regulated atrophic events, termed thymic involution, followed by subsequent regrowth. This involution can be temporally induced by stress stimuli such as infection and pregnancy, processes for which the molecular mechanisms are relatively well described [11]. A chronic form of involution also occurs with age, a phenomenon highly conserved among vertebrates [12]. During age-related thymic involution the functional output of the thymus is progressively lost over time, irreversible bar several effective transient treatments [13]. This age-related thymic involution is thought to be a major contributor to the degeneration of effective immunity in older persons. The decline in T-cell output can be partially compensated for by homeostatic expansion of preexisting peripheral T cells, however this process leads to a reduction in TCR repertoire, with diminished responsiveness to new antigens as a consequence [14]. These age-related defects in T cells are the major contributor to the defective responses to vaccines that develop with age [15, 16], a process that imposes a significant medical burden upon older persons [17]. Despite the medical importance of age-related thymic involution, the cellular mechanisms remain poorly defined. The decline in thymic output has been associated with a number of major disruptions to thymic architecture, while the proportion of thymocyte subsets remains largely unaffected, with the notable exception of reduced pro-T-cell numbers [18, 19]. This has led to the structure-led model of thymic involution, where epithelial-originating changes drive involution [20–22]. However, dissecting the causality of events is complicated by the slow progression of the changes and by the influence of stromal defects on thymocytes and vice versa [23, 24]. As a further complication, many of the age-related changes observed may be extraneous to the development of functional defects.

Despite the protracted nature of age-related thymic involution, there is variation in the rate of involution, both within mice and humans. In particular, FVB/N mice undergo thymic involution at an earlier time point and in a more rapid fashion than C57BL/6 mice [25]. Here we have taken advantage of this inter-strain variation in age-related thymic involution to study the relationship between stromal and hematopoietic changes, and to discern the causative processes of thymic involution. We identified

both shared and distinct structural and architectural changes to the stroma that precede thymic involution in the two strains, as well as a shared degeneration in pro-T-cell precursor number prior to involution. Genetic and compartment analysis of these traits demonstrated the stromal age-dependent changes to be only correlative to thymic involution, with the causative change being the independent phenotype of hematopoietic-intrinsic decline in pro-T-cell precursor number.

## Results

### The FVB/N thymus displays altered thymic architecture prior to premature involution

The FVB/N mouse strain has been previously characterized to undergo premature thymic involution, with a sharp decrease in cellularity and disruption of the cortico-medullary junction as early as 5 months, compared to 12–15 months in C57BL/6 mice [25]. As the differential timing of thymic involution between the FVB/N and C57BL/6 strains allows the segregation of generic age-dependent changes from the functional changes that drive chronic involution, we investigated this phenomenon further. C57BL/6 mice reached peak thymus cellularity at 4 weeks, after which a slow decline in cellularity was initiated, reaching involuted status at around 1 year of age (Fig. 1A). FVB/N mice displayed a similar thymic cellularity at 4 weeks, but the decline in cellularity was far more rapid than C57BL/6 mice, with the thymus being involuted by 16 weeks of age (Fig. 1A). From the neonatal stage, the FVB/N thymus demonstrated altered thymic architecture, with “cauliflower-shaped” fibroblast-lined invaginations budding in from the thymic surface into the interior, unlike the smooth surface of the C57BL/6 thymus (Fig. 1B). Apart from the invaginations, the FVB/N thymus was structurally normal at birth, with discrete cortical/medullary development and normal localization of epithelial subsets, endothelium, dendritic cells, macrophages, and thymocytes (Supporting Information Fig. 1). The invaginations observed in the FVB/N thymus at the neonatal stage were further developed by 4 weeks of age, at which point the invaginations apparently bisected the thymic lobe into multiple lobules (Fig. 1B). The opening of the invaginations could be observed on the surface of the FVB/N thymus, as revealed by the accumulation of topically applied crystal violet dye, while these features were almost absent on the surface of C57BL/6 age-matched control thymus (Fig. 1C). In order to further assess the structural changes at the surface, thymic tissue was analyzed using scanning electron microscopy. High-resolution images showed the C57BL/6 thymus to be topologically barren, apart from the division between thymic lobes, while the FVB/N thymus revealed additional surface fissures, distinct from the separation of thymic lobes in that the fissures were interconnected by a fibrous network (Fig. 1D). With age, these invaginations supported adipocyte growth, with adipocytes being limited to the capsular region in the C57BL/6 thymus, while growing in these invaginations in FVB/N thymus (Supporting Information Fig. 2).

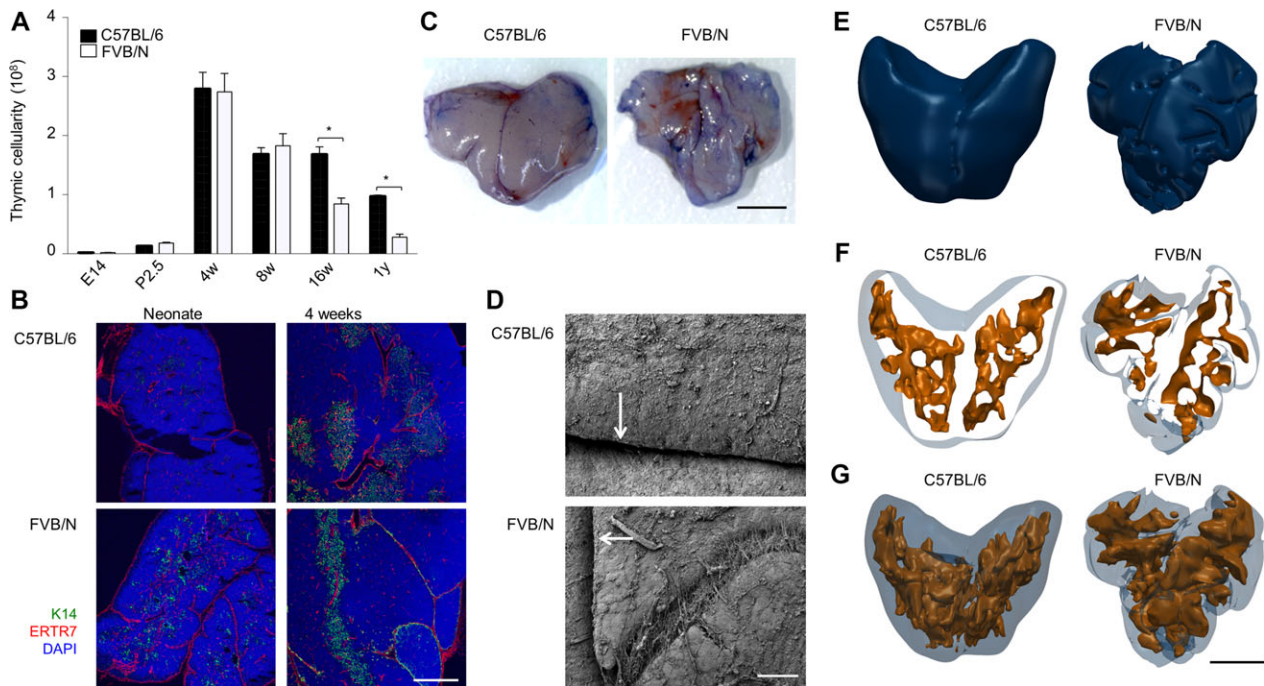


**Figure 1.** Altered thymic architecture precedes thymic involution in FVB/N mice. (A) Thymic cellularity from C57BL/6 and FVB/N mice at embryonic day E14; neonate day P2.5; and time points 1, 2, 4, and 12 months was measured by cell enumeration. Bars show results pooled from five individual experiments with 4–20 mice per group as mean  $\pm$  SEM,  $p < 0.05$ , Student's *t*-test. (B) Immunofluorescent staining of the thymus of C57BL/6 and FVB/N mice assessed at birth (P2.5) and 4 weeks of age. Representative pictures from three mice are shown. Keratin 14 (mTEC, green), ERTR7 (fibroblasts, red), and DAPI (blue). Scale bar represents 250  $\mu$ m. (C) Representative photographs of C57BL/6 and FVB/N thymi at 4 weeks of age, following topical application of crystal violet to highlight surface invaginations. Representative results of three experiments (one mouse per group). Scale bar represents 5 mm. (D) Representative scanning electron micrograph of C57BL/6 and FVB/N thymi at 4 weeks of age. Arrow indicates gap between thymic lobes. Representative results of three experiments (one mouse per group). Scale bar represents 100  $\mu$ m. (E–G) The thymus of 4-week-old C57BL/6 and FVB/N mice was reconstructed into a 3D structure following serial sectioning. Scale bar represents 5 mm. (E) Surface topography of the C57BL/6 and FVB/N thymi, including invaginations originating from the surface. (F) Location of medullary islets within the thymi of C57BL/6 and FVB/N mice, bisected. (G) Overlay of surface topography with medullary islets.

The bisection of the FVB/N thymus by invaginations apparently fractionated the thymic medulla into multiple functional units. In order to determine whether this 2D bisection extended into three dimensions, we reconstructed a 3D model of both the C57BL/6 (Supporting Information Movie 1) and FVB/N thymi (Supporting Information Movie 2) from serial sections. Reconstruction demonstrated that while the invaginations of the FVB/N

thymus reached deep into the interior of the thymus they did not bisect the thymus in three dimensions (Fig. 1E and F). Furthermore, the thymic medulla remained a contiguous islet in FVB/N mice, with regions seemingly divided by invaginations in 2D sections rejoining in 3D space (Fig. 1F and G and Supporting Information Movie 2). These features demonstrate an anatomical disparity between the FVB/N and C57BL/6 strains present during

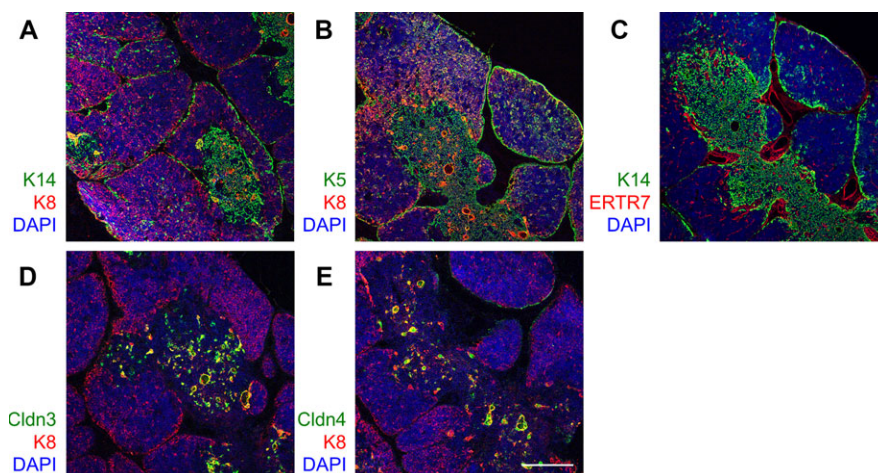


**Figure 2.** Surface invaginations analogous to FVB/N mice are present in human thymus samples. Immunofluorescent staining of human thymus samples. (A) Keratin 14 (mTEC, green), Keratin 8 (epithelium, red), and DAPI (blue). (B) Keratin 5 (mTEC, green), Keratin 8 (epithelium, red), Keratin 5 (mTEC, green), and DAPI (blue). (C) Keratin 14 (mTEC, green), ERTR7 (fibroblasts, red), and DAPI (blue). (D) Claudin 3 (mTEC subset, green), Keratin 8 (epithelium, red), and DAPI (blue). (E) Claudin 4 (mTEC subset, green), Keratin 8 (epithelium, red), and DAPI (blue). One representative picture from serial sections of three individuals is shown. Scale bar represents 250  $\mu$ m.

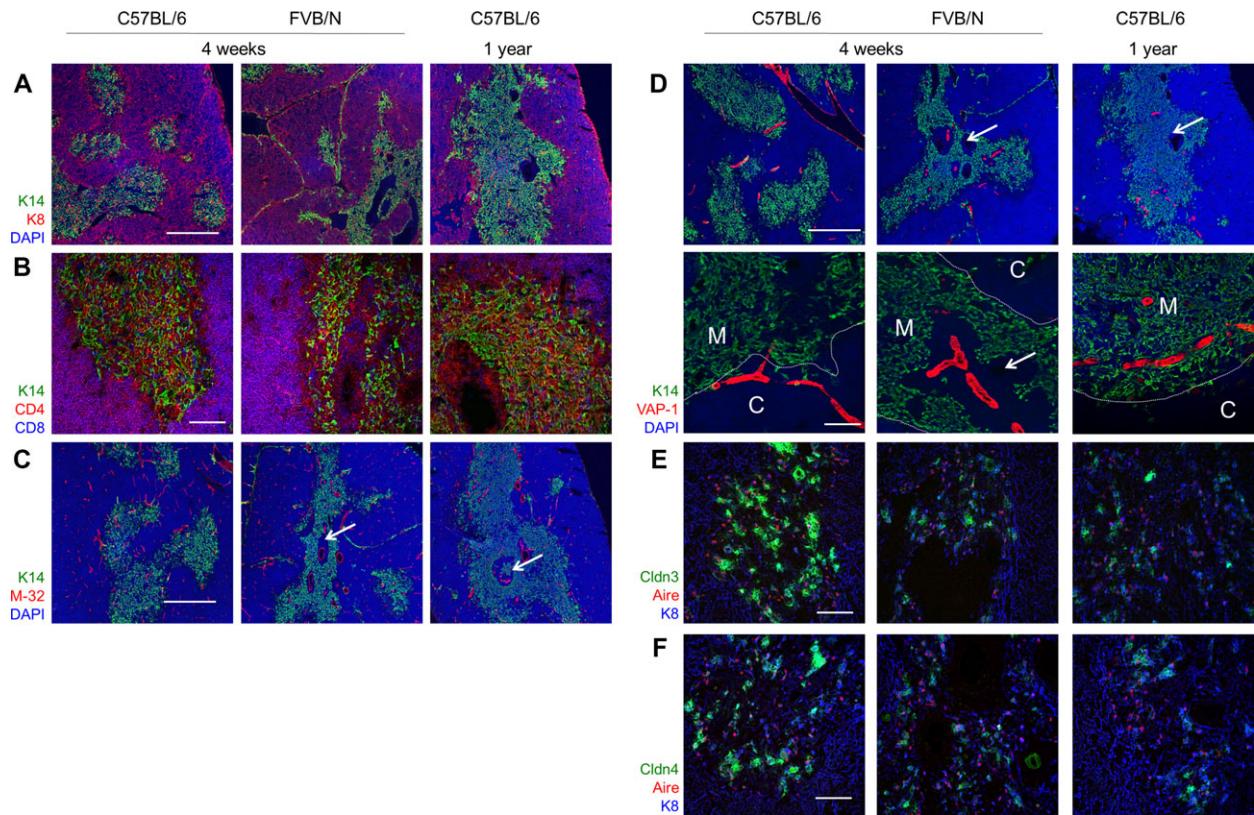


**Figure 3.** Premature development of epithelial voids surrounding thymic vasculature in FVB/N mice. Immunofluorescent staining of the thymus of C57BL/6 and FVB/N mice assessed at 4 weeks of age and C57BL/6 mice at 1 year of age. Representative pictures from more than three mice are shown. Arrows indicate epithelial voids. (A) Keratin 14 (mTEC, green), Keratin 8 (epithelium, red), and DAPI (blue). Scale bar represents 250  $\mu\text{m}$ . (B) Keratin 14 (mTEC, green), CD4 (red), and CD8 (blue). Scale bar represents 50  $\mu\text{m}$ . (C) Keratin 14 (mTEC, green), MECA-32 (endothelium, red), and DAPI (blue). Scale bar represents 250  $\mu\text{m}$  (upper) and 50  $\mu\text{m}$  (lower). Cortex (C) and medulla (M) are represented on the lower panel, with cortical–medullary junction indicated by dashed line. (D) Keratin 14 (mTEC, green), VAP1 (endothelium subset, red), and DAPI (blue). Scale bar represents 250  $\mu\text{m}$  (upper) and 50  $\mu\text{m}$  (lower). (E) CLDN3 (mTEC subset, green), Aire (mTEC subset, red), and Keratin 8 (epithelium, blue). Scale bar represents 50  $\mu\text{m}$ . (F) CLDN4 (mTEC subset, green), Aire (mTEC subset, red), and Keratin 8 (epithelium, blue). Scale bar represents 50  $\mu\text{m}$ .

early development, consistent with a structure-led model of thymic involution. It is notable that in terms of basic thymic architecture, the invaginations of lobular FVB/N thymus, although different in scale, are phenotypically closer to the complex infant human thymus (Fig. 2) than to the simplistic structure of the C57BL/6 thymus.

### Iterative disruption of the epithelial–endothelial relationship in FVB/N mice

Despite the striking disparity in ultrastructure between the C57BL/6 and FVB/N neonatal thymi, expansionary growth during the neonatal period was unaffected (Fig. 1A), indicating that the thymic invaginations were not responsible for a primary failure in thymic sustenance. We therefore performed an in-depth comparative histological analysis at 4 weeks of age, a time point before divergence between C57BL/6 and FVB/N thymic cellularity begins. In addition to the invaginations described above from the neonatal stage onwards, by 4 weeks the FVB/N mouse developed an additional feature, that of unstructured regions devoid of

thymic epithelium, but still cellular in composition (Fig. 3A). These “epithelial voids” occurred exclusively in the medulla, as they were surrounded by medullary thymic epithelium and were filled with CD4 and CD8 single-positive thymocytes (Fig. 3B). Epithelial voids frequently formed around the thymic vasculature (Fig. 3C), and in particular the formation of the epithelial voids resulted in displacement of VAP-1<sup>+</sup> endothelium from the cortical–medullary border to within epithelial voids distant from the cortex (Fig. 3D). These changes were analogous to the enlargement of the perivascular space that occurred in aged C57BL/6 mice (Fig. 3A–D), suggesting a conserved underlining mechanism between premature thymic involution in FVB/N mice and aged thymic involution in C57BL/6 mice. Beyond the development of epithelial voids and the displacement of the VAP-1<sup>+</sup> endothelium, few changes were observed between the FVB/N and C57BL/6 thymi, with normal distribution of epithelial subsets and nonepithelial cellular constituents (Supporting Information Fig. 3). The only notable exception was the downregulation of Claudin 3 and Claudin 4 in the medulla of FVB/N mice at 4 weeks of age – a phenotype also observed at the time point 1 year in C57BL/6 mice and hence preceding thymic involution in both strains (Fig. 3E and F).

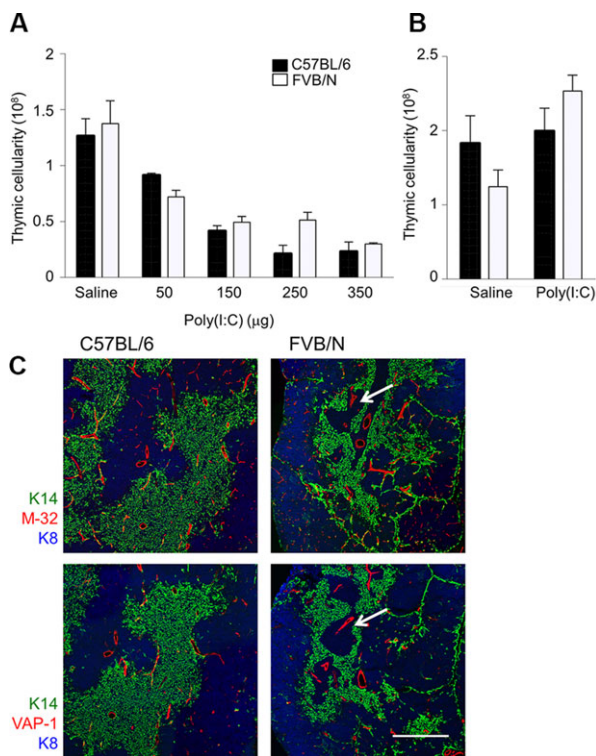


**Figure 4.** Structural abnormalities of the FVB/N thymus are iterative in nature and do not alter sensitivity to IFN- $\alpha$ -mediated thymic involution. (A) Six-week-old C57BL/6 and FVB/N mice were injected with 0–350  $\mu$ g poly(I:C) on days 0 and 3, prior to analysis of thymic cellularity by cell enumeration on day 4. Bars show mean  $\pm$  SEM pooled from two to three mice per dose. Representative results of two individual experiments are shown. (B) Recovery of C57BL/6 (black bars) and FVB/N (white bars) mice 21 days following injection at 6 weeks of age with 300  $\mu$ g poly(I:C) on days 0 and 3. Thymic cellularity was analyzed by cell enumeration. Bars show mean  $\pm$  SEM pooled from four to five mice per dose,  $p < 0.05$ , Student's *t*-test. Representative results of two individual experiments are shown. (C) Representative immunofluorescent staining for Keratin 14 (mTEC, green), Keratin 8 (epithelium, blue), and MECA-32 (endothelium, red) or VAP1 (endothelium subset, red) on C57BL/6 and FVB/N thymi on day 21 post poly(I:C) treatment. Representative pictures from more than three mice are shown. Scale bar represents 100  $\mu$ m.

In order to determine whether the structural changes observed affect age-related involution only, or whether they also predispose the FVB/N mouse to hypersensitivity to thymic involution in response to other stimuli, young C57BL/6 and FVB/N mice were challenged with a titration of involution-inducing substrate. A titration of poly(I:C) was previously used to identify hypersensitivity to IFN- $\alpha$ -mediated involution, as susceptible genetic backgrounds show increased involution at lower doses [26]. Both C57BL/6 and FVB/N mice showed a dose-dependent involution response, with no substantive differences in sensitivity (Fig. 4A) or regrowth (Fig. 4B). Histological analysis of the regrown thymi of both C57BL/6 and FVB/N mice, revealed that reconstitution of the FVB/N thymus did not correct the anatomical features of thymic invaginations or epithelial voids (Fig. 4C), demonstrating the development of these features is not restricted to initial organogenesis and, rather, is iteratively reproduced in subsequent

developmental rounds. Together these results suggest that the thymic changes caused by the FVB/N genetic background drive a true age-related thymic involution process, rather than increasing a general propensity to thymic degradation.

### Thymic architectural changes are controlled by weak polygenic effects

In order to dissect the genetic control over the thymic architectural changes described above, a high-throughput immunohistochemical screening panel was developed (Fig. 5A). Two-color immunohistochemistry using a medullary epithelium marker (Keratin 14) and a pan-endothelial marker (MECA-32) allowed quantification of the number of invaginations (defined as a fissure of greater than 400  $\mu$ m length originating at the surface) and epithelial voids (defined as Keratin 14<sup>-</sup> regions of greater than 150  $\mu$ m diameter, surrounded by Keratin 14<sup>+</sup> tissue). Imposition of these criteria on the parental strains and a (C57BL/6xFVB/N).F1 intercross identified a near-absence of these features in the C57BL/6 thymus and the common appearance in both FVB/N and (to a lesser extent) F1 intercross mice, indicating a semidominant FVB/N trait (Fig. 5B and C). To dissect the genetic control over altered thymic architecture between the C57BL/6 and FVB/N mouse strains, a cohort of >133 (C57BL/6xFVB/N).F2 was run through the immunohistochemical screening panel. The number of thymic invaginations and medullary epithelium voids was assessed and mice were genotyped at 491 informative SNP-based markers, providing genome-wide origin data at an average resolution of 3 cM. Genome-wide linkage to the number of invaginations gave no significant linkage (Fig. 5D), although several loci showed weak effects, indicating polygenic control over the traits. Genome-wide QTL analysis identified linkage of the number of epithelial voids to two loci, one on chromosome 7 (Fig. 5E), centered on the rs31944466 SNP located at 31 cM (Fig. 5F), and one on chromosome 14, centered on the rs30160834 SNP located at 61.4 cM (Fig. 5G). Individually these loci accounted for only 7–15% of the phenotypic variation, a value highly dependent on the definition of an epithelial void used, demonstrating a highly polygenic trait. Notably, FVB/N variants were not exclusively responsible for the development of epithelial voids; indeed, while the rs31944466 SNP linkage to epithelial voids was caused by FVB/N genotypes (Fig. 5H), the rs30160834 SNP linkage was caused by C57BL/6 genotypes (Fig. 5I). These results indicate that rather than being an abnormality of FVB/N mice, these changes to the thymic architecture are encoded within the genomes of both mouse strains, with complex polygenic control driving earlier manifestation in FVB/N mice.

### Premature thymic involution is linked to reduced pro-T cells

Together, these results support the structure-led model of thymic involution, whereby the degradation of the architectural integrity of the thymus leads to reduced function. In particular, the thymus

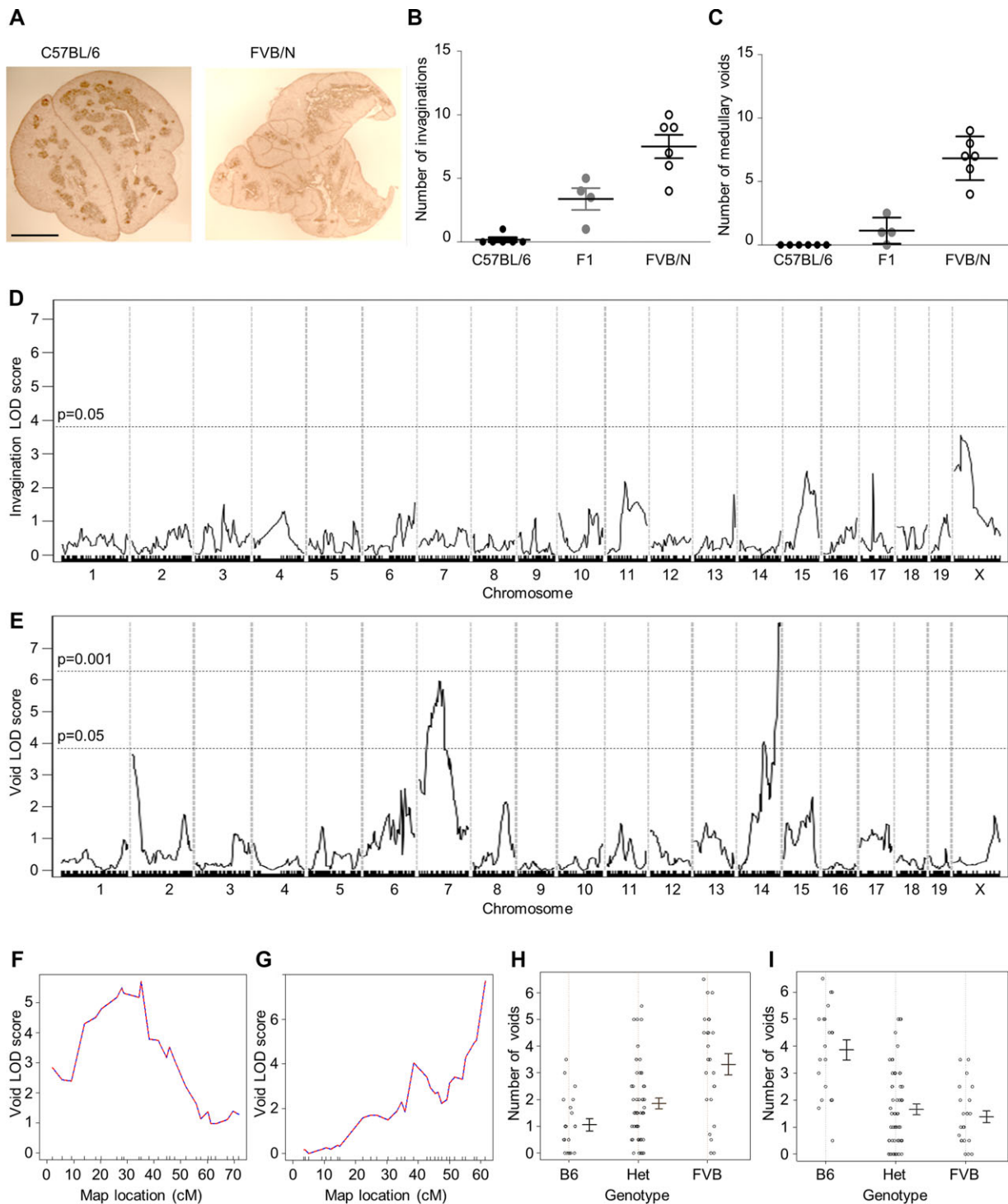


**Figure 5.** Weak polygenic effects control changes in thymic architecture in C57BL/6 and FVB/N mice. (A) Representative immunohistochemical staining of 4-week-old C57BL/6 and FVB/N mice for Keratin 14 (brown) and MECA-32 (red). One representative image from serial sections from six mice is shown. Scale bar represents 3 mm. (B) Average number of thymic invaginations greater than 400  $\mu\text{m}$  and (C) epithelial voids larger than 150  $\mu\text{m}$  diameter in C57BL/6, FVB/N, and (C57BL/6  $\times$  FVB/N).F1 mice at 4 weeks of age. Each symbol represents an individual mouse, bars show mean  $\pm$  SEM from four to six mice per group. (D) Genome-wide LOD scores showing the linkage to the number of thymic invaginations. (E) Genome-wide LOD scores for linkage to the number of epithelial voids in (C57BL/6  $\times$  FVB/N).F2 mice as determined by standard interval mapping (blue) and extended Haley–Knott regression (red). Dashed lines indicate the 95th confidence percentile in 1000 randomized linkage runs. (F) Chromosome 7 and (G) chromosome 14 LOD scores for linkage to the number of epithelial voids in (C57BL/6  $\times$  FVB/N).F2 mice. (H) Genotype–phenotype association between chromosome 7 rs31944466 SNP and the number of epithelial voids. (I) Genotype–phenotype association between chromosome 14 rs30160834 SNP and the number of epithelial voids. Each symbol represents one mouse from 133 mice, with confidence interval, as determined by standard interval mapping on R/QTL.

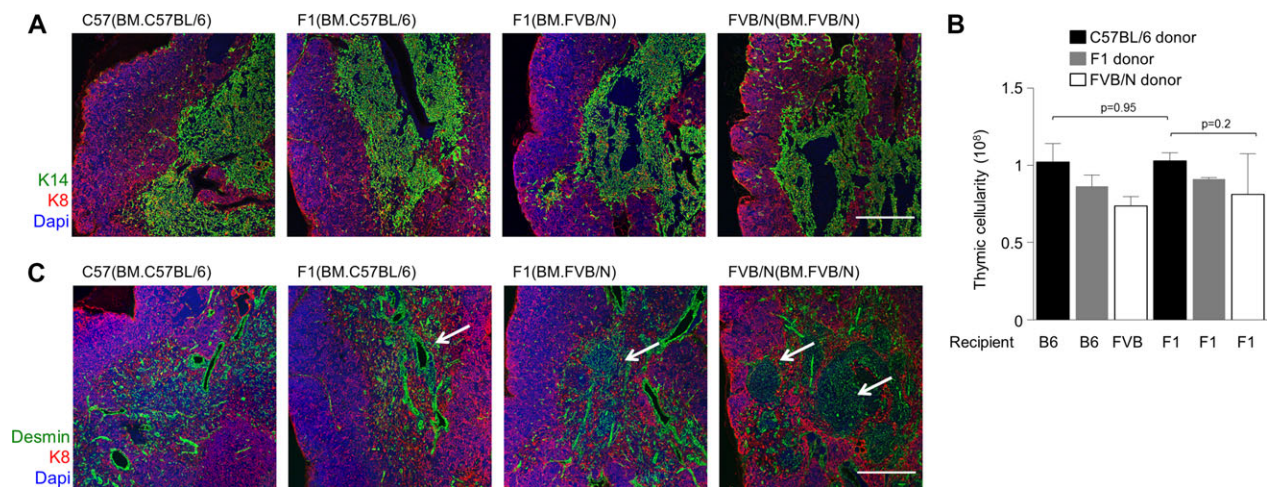


**Figure 6.** Changes in thymic architecture are neither necessary nor sufficient for premature thymic involution. (A) BM chimeras were generated by reconstituting C57BL/6, FVB/N, or (C57BL/6x FVB/N).F1 recipients with C57BL/6 or FVB/N BM. Twenty weeks after reconstitution, the thymus was removed and assessed for structural changes. Representative immunofluorescent staining for Keratin 14 (mTEC, green), Keratin 8 (epithelium, red), and DAPI (blue). Representative pictures from more than three mice are shown from three to eight mice per group. Scale bar represents 3  $\mu$ m. (B) BM chimeras were generated by reconstituting C57BL/6, FVB/N, or (C57BL/6x FVB/N).F1 recipients with C57BL/6, FVB/N, or (C57BL/6x FVB/N).F1 BM. Twenty weeks after reconstitution, the thymus was removed and assessed for cellularity by cell enumeration. Bars show mean  $\pm$  SEM pooled from three to eight mice per group, *p* values listed, Student's *t*-test. Representative results of two individual experiments are shown. (C) Immunofluorescent staining of the thymus of BM chimeras was generated by reconstituting C57BL/6, FVB/N, or (C57BL/6x FVB/N).F1 recipients with C57BL/6 or FVB/N BM, as in (A). Arrows indicate epithelial voids. Desmin (green), Keratin 8 (epithelium, red), and DAPI (blue). Representative pictures from more than three mice are shown. Scale bar represents 3  $\mu$ m.

is critically dependent on the continual import of progenitor T cells from the BM via the specialized VAP-1<sup>+</sup> postcapillary venules at the cortico-medullary junction [27, 28]. The disconnection between VAP-1<sup>+</sup> endothelium and thymic epithelial cells that develops in aged C57BL/6 mice suggests that the loss of contact between epithelium and endothelium may reduce the entry signals required for progenitor T cells to enter from the blood stream, a model supported by reduced numbers of pro-T cells in the aged C57BL/6 thymus [29]. Under this model, the influence of multiple genetic polymorphisms on the FVB/N background would hasten the development of these architectural features, resulting in premature age-related thymic involution. Due to the complexity of genetic control confounding further analysis via this route, we undertook further compartment analysis to test whether the structural changes were directly linked to thymic involution. To determine whether the trait was intrinsic to the hematopoietic or nonhematopoietic compartment, F1 mice were reconstituted with BM from the C57BL/6 or FVB/N parent strain and were analyzed for the presence of thymic invaginations and epithelial voids. The chimeric F1 mice demonstrated “FVB-like” thymic architecture regardless of the BM source, indicating that the causative loci affect the phenotypic difference via the thymic stroma (Fig. 6A). To track the compartment responsible for premature thymic involution, we generated additional sets of BM chimeras, including C57BL/6, FVB/N, and F1 mice reconstituted with C57BL/6, FVB/N, or F1 BM (Fig. 6B). FVB/N mice reconstituted with FVB/N BM showed reduced thymic cellularity at 20 weeks post reconstitution compared to C57BL/6 mice reconstituted with C57BL/6 BM, demonstrating that irradiation and reconstitution do not impede premature thymic involution. However, assessment of the

other chimeric conditions clearly demonstrated that premature thymic involution was controlled by hematopoietic factors, as the thymic cellularity of F1 mice reconstituted with C57BL/6 BM was indistinguishable from reconstituted C57BL/6, while F1 mice reconstituted with FVB/N BM demonstrated reduced thymic cellularity (Fig. 6B). The capacity for the (C57BL/6x FVB/N).F1 stroma to support thymopoiesis when reconstituted with C57BL/6 BM is perplexing, due to the loss of epithelial–endothelial interaction described above. However this spatial dislocation may be compensated for by other factors, such as the enrichment of epithelial voids for desmin (Fig. 6C) and the structural protein allowing long-distance communication to endothelial cells in LNs [30]. These results clearly demonstrate that the altered thymic structure associated with aging is neither necessary nor sufficient for thymic involution, with premature thymic involution in FVB/N mice being controlled by hematopoietic factors.

Due to the hematopoietic-intrinsic control over premature thymic involution in the FVB/N strain, we performed a comparative analysis of thymocyte differentiation between C57BL/6 and FVB/N mice. At the late embryonic stage, C57BL/6 and FVB/N mice contained equivalent numbers of the earliest-known thymic progenitor cell, pro-T cells (Fig. 7A and B, Supporting Information Fig. 4). A 50% decrease was apparent after birth, while at 4 weeks of age, the FVB/N thymus revealed a striking 80% decrease in the frequency of pro-T cells (Fig. 7A and B). This defect in pro-T cells became even more striking with age, with the FVB/N thymus being completely deficient in CD117<sup>hi</sup> pro-T cells by 16 weeks of age, while this population was clearly detectable in C57BL/6 mice out to 1 year (Fig. 7A and B). This deficiency in pro-T cells was not

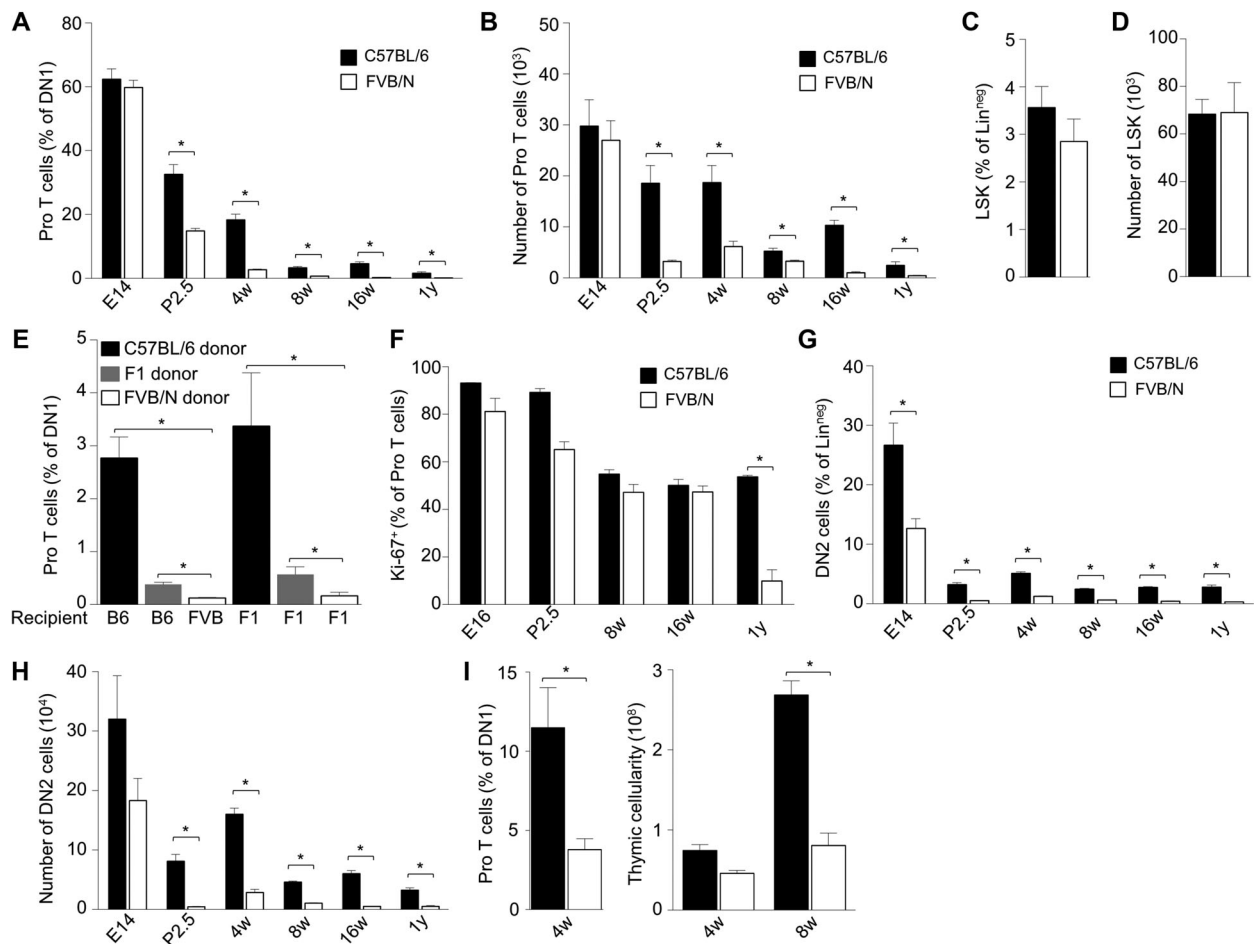


**Figure 7.** Reduced entry of progenitor T cells into the FVB/N thymus. (A) Percentage and (B) absolute number of Lin<sup>neg</sup> CD117<sup>hi</sup> DN1 (pro-T cells) in C57BL/6 and FVB/N mice at day 14 of embryonic development (E14); neonatal stage (P2.5); and 4, 8, and 16 weeks and 1 year of age. Bars show results pooled from five individual experiments with three to ten mice per group as mean  $\pm$  SEM as determined by flow cytometry. (C) Percentage and (D) absolute number of Lin<sup>neg</sup> CD117<sup>+</sup> Sca1<sup>+</sup> LSK cells in C57BL/6 (black bars) and FVB/N (white bars) BM at 16 weeks of age as determined by flow cytometry. Bars show mean  $\pm$  SEM pooled from five mice per group. Representative results of two individual experiments are shown. (E) BM chimeras were generated by reconstituting C57BL/6, FVB/N, or (C57BL/6 $\times$ FVB/N).F1 recipients with C57BL/6, FVB/N, or (C57BL/6 $\times$ FVB/N).F1 BM. Twenty weeks after reconstitution, the thymus was removed and assessed for the percentage of pro-T cells by flow cytometry. Bars show mean  $\pm$  SEM pooled from three to eight mice per group. Representative results of two individual experiments are shown. (F) Ki67 expression in pro-T cells from C57BL/6 and FVB/N thymi at day 16 of embryonic development (E16), neonatal stage (P2.5), and 8 and 16 weeks and 1 year of age as determined by flow cytometry. Bars show mean  $\pm$  SEM pooled from three to ten mice per group from four individual experiments. (G) Percentage and (H) absolute number of DN2 cells from C57BL/6 (black bars) and FVB/N (white bars) thymi at day 14 of embryonic development (E14); neonatal stage (P2.5); and 4, 8, and 16 weeks and 1 year of age as determined by flow cytometry. Bars show mean  $\pm$  SEM pooled from three to ten mice per group from five individual experiments. (I) C57BL/6 mice were irradiated and reconstituted with either 20% Ly5.1 BM and 80% C57BL/6 BM ("100% viable precursors," black bar), or 20% Ly5.1 BM and 80% C57BL/6.Rag<sup>-/-</sup> BM ("20% viable precursors," white bar). Bars show mean  $\pm$  SEM pooled from four to five mice per group. Representative results of two individual experiments are shown. (Left) Pro-T-cell numbers at 4 weeks of age. (Right) Total thymic cellularity at 4 and 8 weeks post reconstitution. \* $p < 0.05$ , Student's *t*-test.

reflected in the immediate BM stem and progenitor cells, the Lin-Sca-1+c-Kit+ (LSK) cells, as numbers were equivalent between C57BL/6 and FVB/N mice at 16 weeks of age (Fig. 7C and D).

To determine whether the reduction in pro-T cells was dependent on the stromal changes, and hence merely correlative with thymic involution, we determined the compartmental control over this trait using the BM chimera approach used before. Assessment of pro-T-cell numbers in BM chimeric mice demonstrated that the low number of pro-T cells in FVB/N thymi was due to hematopoietic-intrinsic factors (Fig. 7E). Strikingly, this means that an F1 thymus reconstituted with C57BL/6 BM has the

architectural abnormalities of the FVB/N thymus (Fig. 6A), but normal pro-T-cell number (Fig. 7E) and total thymic cellularity (Fig. 6B). Analysis of pro-T cells within the C57BL/6 and FVB/N mice revealed normal levels of proliferation (Fig. 7F), suggesting that reduced numbers were not due to differential expansion in situ, but rather due to reduced recruitment. Evaluation of CCL21 and CCL25, important ligands for pro-T-cell recruitment, revealed increased expression by TECs in FVB/N mice, however the receptor CCR7 was decreased on FVB/N DN1 T cells, consistent with a recruitment defect (Supporting Information Fig. 5). Beyond the DN1 stage, a decline of DN2 cells was also observed in FVB/N mice,

but with different kinetics, being reduced from the late embryonic stage followed by progressive loss from birth (Fig. 7G and H), a phenotype associated with aging in other strains [31]. By contrast, later stages of thymocyte differentiation appeared relatively intact, with changes within the DN population not affecting the number of DP cells generated and no defect in either  $\beta$ -selection or positive selection (Supporting Information Table 1). Due to the proliferative nature of DN T cells, experimental testing was required to determine whether a reduction of this nature would be rate limiting for maintained thymic cellularity. We therefore generated a mixed BM chimera system, where the number of BM precursors capable of developing past the DN stage was limited by 80%, by reconstituting an irradiated C57BL/6 mouse with either 100% competent BM (20% C57BL/6.Ly5.1, 80% C57BL/6) or 20% competent BM (20% C57BL/6.Ly5.1, 80% C57BL/6.Rag<sup>-/-</sup>). This system resulted in a reduction of thymic pro-T cells by 80% (Fig. 7I), recapitulating the FVB/N defect, albeit by a different mechanism. Analysis of the thymic cellularity of these chimeras demonstrated that, independent of the FVB/N background, the reduction in thymic pro-T-cell numbers resulted in a more rapid involution of the thymus (Fig. 7I). Together, these results demonstrate that a reduction in pro-T-cell numbers, while correlative with thymic architectural changes, is under independent control. Furthermore, the thymic architectural changes are neither necessary nor sufficient to drive thymic involution, while the independent loss of pro-T cells is sufficient to precipitate premature thymic involution.

## Discussion

The involution of the thymus with age is postulated to be one of the significant immunodegenerative events driving reduced immune function in the elderly [17]. Despite the potential importance of age-dependent thymic involution for healthy aging, dissecting the mechanism by which the thymus involutes has been problematic as a myriad of phenotypic changes gradually occur with aging, of which the majority are likely to be noncausative. By analyzing thymic involution in the FVB/N mouse strain, in which age-dependent thymic involution is initiated prematurely, we were able to dissociate those components of thymic change that are common to thymic involution in both the aged C57BL/6 mouse and the young FVB/N mouse. Several age-dependent phenotypes observed in the C57BL/6 thymus and proposed as causative events in thymic involution were not observed in the FVB/N thymus prior to involution – for example, the disorganization of the cortico-medullary junction [32], the increase in adipocytes [33], and the shift from immature (p63) to mature (Keratin 10) epithelial markers. While not excluding the possibility that age-dependent thymic involution follows mechanically distinct pathways in these two mouse strains, parsimony would suggest that these age-dependent changes are not required for involution to occur. Conversely, we described here a major structural difference in the FVB/N mouse strain, which by the same rationale is unlikely to be the driver in premature thymic involution.

This structural difference is the neonatal development of surface invaginations in FVB/N mice. These invaginations are fibroblast lined, are tightly bound by extracellular matrix, and provide the scaffold upon which adipocytes grow with age. While these invaginations divide the thymus into multiple lobules, interconnections between the epithelial components of each lobule are maintained, creating a single functional unit. It is notable that in terms of basic thymic architecture, the lobular FVB/N thymus with invaginations and epithelial voids is phenotypically closer to the complex human thymus than to the simplistic structure of the C57BL/6 thymus.

In addition to excluding a number of strong stromal phenotypes from active participation in age-dependent thymic involution, we found here two key phenotypes that are shared between age-dependent thymic involution in the C57BL/6 and FVB/N strains – namely the development of epithelial voids and the reduction in pro-T-cell numbers. In both strains, the development of epithelial voids and the reduction in pro-T-cell numbers predated the thymic involution – with earlier and rapid development in FVB/N mice and slower progressive development in C57BL/6 mice. The structure-led model of thymic involution would predict these two phenotypes to be causatively linked, with the development of epithelial voids breaking the connection between thymic epithelial cells and the VAP-1<sup>+</sup> vasculature required for the entry of BM-derived precursors [27, 28]. Indeed, in an isolated in vitro system, the addition of thymic epithelial cells to an endothelial-cell culture doubles the capacity of the endothelium to bind thymic progenitors [34]. It was thus attractive to speculate that the spatial dislocation of epithelium and endothelium would reduce the efficiency of precursor entry.

Despite the appeal of the structure-led hypothesis for age-related thymic involution, our results here demonstrate that the epithelial void formation and other stromal-dependent phenotypes are aging epiphenomena, which are neither necessary nor sufficient for thymic involution to take place. This analysis also rules out participation of *Skint-1* mutation, recently found to alter  $\gamma\delta$  T-cell selection in FVB/N mice in a stromal-dependent fashion [35, 36]. By contrast, the primary decline in the number of pro-T cells is strongly implicated as the causative mechanism of thymic involution, with both pro-T-cell number and premature thymic involution being controlled by the hematopoietic compartment, and experimental restriction in the number of functional pro-T cells recapitulating the involution phenotype. Two salient points derive from this observation. First and foremost, this study suggests that further investigation into the mechanisms of age-related thymic involution focus on the hematopoietic stem cell compartment, in which several changes are known to occur with age [37, 38]. We currently lack a good understanding of the phenotype of the blood-borne precursor cell (thymus-settling progenitor, TSP) that lies between the BM LSK cell and the thymus pro-T cell [39]. It is, however, this unknown cell type that is the key candidate for premature involution in FVB/N mice, as the LSK precursor remains normal in number, while the pro-T cell is dramatically lower, despite normal proliferation. These results suggest that either emigration or immigration of the blood-borne precursor constitutes the restriction point that limits thymocyte

number and drives thymic involution. The delay between the reduction in pro-T cells and thymic involution in this setting may reflect the capacity of sustained proliferation of pro-T cells in the absence of fresh competitors [7]. Second, these results point to a remarkable degree of versatility in thymic structure, whereby BM precursor entry and latter differentiation are highly robust despite the diversity of architecture observed between mouse strains (and, indeed, the human thymus). In particular, the unimpeded entry and differentiation of C57BL/6 pro-T cells in the (C57BL/6xFVB/N).F1 thymus, riddled with epithelial voids, suggests that thymic fibroblasts are able to fulfil local microstructure requirements in the absence of medullary thymic epithelial cells. The function of thymic fibroblasts has been little studied; however loss of fibroblasts from a thymic graft results in an involuted thymus [40]. We speculate that part of the unappreciated function of fibroblasts in compensating for local epithelial absence may be in the production of a comprehensive desmin lattice spanning the epithelial voids, analogous to the LN function [30]. In light of these findings, we would propose that the young C57BL/6 thymus should not be considered the “normal” thymus and the features of the FVB/N or aged C57BL/6 thymus should not be considered “abnormal” or “defective.” With a similar capacity to support the key restriction point of thymic function (precursor entry), it may be more correct to consider the thymus an organ capable of a diverse array of functionally equivalent structures, complete with invaginations, adipocyte enclaves, cysts, and epithelial voids. Using this perspective, the young C57BL/6 thymus is simply an example of the most simplistic structure, resulting from the interaction of multiple pro- and anticomplexity loci. This perspective also solves the problematic observation that the human thymus has a much greater complexity of structure than even the aged C57BL/6 thymus, even when assessed at birth, despite having a high functional potential.

## Materials and methods

### Patient samples

Human thymi removed during cardiac surgery were collected from children 0–6 months of age at the Sahlgrenska University Hospital, Gothenburg, Sweden. The tissue was immediately snap frozen using Tissue-Tek Optimum Cutting Temperature (O.C.T.) compound (Sakura, Torrance, California). Parents gave informed consent, and the study was approved by the local ethics committee (no. 217-12, 2012-04-26).

### Mice

C57BL/6 mice were obtained from Charles River Laboratory. FVB/N mice [41] were obtained from Taconic farms and were intercrossed on the C57BL/6 background to generate F1 and F2 offspring. C56BL/6.*Rag2*<sup>-/-</sup> mice and C57BL/6.*Ly5.1* con-

genic mice were purchased from Jackson Laboratories. Mice were housed in specific pathogen-free conditions. Equal proportions of male and female mice were maintained throughout the study. High molecular weight poly(I:C) (Invivogen, San Diego, CA, USA) was injected i.p. on days 0 and 3, with cellularity measured on day 4 or 21. BM chimera recipients were lethally irradiated with 9.5 Gray. Donor BM was depleted of T cells by treatment with anti-CD4 (GK1.5, A. Farr) and anti-CD8 (2.43, A. Farr) hybridoma supernatant followed by Low-Tox M rabbit complement (Cederlane, Ontario, Canada) or by anti-CD4- and anti-CD8-biotin staining followed by depletion with streptavidin coupled Dynabeads (Invitrogen, Grand Island, NY, USA), prior to reconstitution of recipients. All experiments were performed in accordance with the University of Leuven Animal Ethics Committee guidelines.

### Flow cytometry

Surface staining for flow cytometry was performed after Fc receptor blocking with 2.4G2 supernatant, using the following reagents (all eBioscience unless otherwise noted): anti-B220-PE-Cy7 (RA3-6B2); anti-CCR7-PE-Cy7 (4B12; 1 h at 37°C after blocking and before staining for other surface markers); anti-CD3-FITC and anti-CD3-PE (145-2C11); anti-CD4-allophycocyanin and anti-CD4-biotin, and anti-CD4-PE-Cy7 (RM4-5); anti-CD8-allophycocyanin and anti-CD8-biotin, anti-CD8-PE, anti-CD8-PE-Cy7, and anti-CD8-PerCP-Cy5.5 (53-6.7); anti-CD19-FITC and anti-CD19-biotin (1D3); anti-CD24-PerCP-Cy5.5 (M1/69), anti-CD25-allophycocyanin, and anti-CD24-PerCP-Cy5.5 (p55); anti-CD44-PerCP-Cy5.5, anti-CD44-PE, and anti-CD44-PE-Cy7 (1M7); anti-CD62L-PE-Cy7 (MEL-14) and anti-CD62L-PerCP-Cy5.5 (H1.2F3); anti-CD117-allophycocyanin (2B8); anti-Foxp3-allophycocyanin (FJK-16s); anti-Gr1-FITC and anti-Gr1-biotin (RB6-8C5); anti-Mac1-FITC and anti-Mac1-biotin (M1/70); anti-Sca1-PE (D1); streptavidin-AlexaFluor647; streptavidin-FITC; anti-TER-119-FITC and anti-TER-119-biotin (TER-119); and anti-TCR $\gamma\delta$ -allophycocyanin and anti-TCR $\gamma\delta$ -biotin (GL3). Following surface staining, cells were fixed with BD fixation/permeabilization buffer (Becton Dickinson, Franklin Lakes, NJ, USA) or treated with the Foxp3 staining kit (eBioscience, San Diego, CA, USA) before staining with anti-Foxp3-allophycocyanin (FJK-16s) and anti-ki67-PE (SolA15). Where required, samples were depleted with anti-CD8 using streptavidin coupled Dynabeads and a “lineage cocktail” consisting of CD4, CD8, CD19,  $\gamma\delta$ -TCR, Mac1, NK1.1, Gr1, and TER-119 was used for exclusion gating. Data was collected on a FACS Canto II flow cytometer (Becton Dickinson) and analyzed using Flowjo (Treestar, Ashland, OR, USA) software version 7.6.5.

### Thymic epithelial cell sorting and quantitative PCR analysis

Thymi from 6- to 8-week-old mice were minced and digested in 1 mL of Liberase TM solution (80 CDU/mL and 40  $\mu$ g/mL

DNaseI in HBSS/10 mM HEPES/1 mM MgCl<sub>2</sub>/1 mM CaCl<sub>2</sub>; Roche, Germany) for three rounds of 20 min at 37°C with continuous rotation. After complete digestion, suspension cells were filtered through 100 μm filter, stained for 1 h at 4°C with anti-CD45-biotin (30F11, eBioscience) followed by depletion with streptavidin-coupled Dynabeads M280 for 60 min at 4°C with continuous rotation (Invitrogen). Cells were stained with anti-BP-1-PE (6C3, eBioscience), anti-EpCAM-PE-Cy7 (G8.8, Biolegend, San Diego, CA, USA), anti-MHCII-PerCP-Cy5.5 (M5/114, Biolegend), anti-UEA-1-FITC (Vector labs, Burlingame, CA, USA), and streptavidin-allophycocyanin-Cy7 before being sorted on a BD FACS Aria III cell sorter. TECs were defined as DAPI<sup>neg</sup>CD45<sup>neg</sup>MHCII<sup>hi</sup>Epcam<sup>+</sup>.

Purified TECs were resuspended into TRIzol and total RNA was isolated using the RNeasy kit (Qiagen, Valencia, CA, USA) and reverse-transcribed with the GoScript reverse-transcription system (Promega, Fitchburg, WI, USA). qPCR was performed on the StepOnePlus (Life Technologies, Carlsbad, USA) with SYBR select master mix (Life Technologies). *Ccl21* and *Ccl25* expression were measured using the primers 5' GTGATGGAGGGGGTCAGGA with 5' GGGATGGGACAGCCTAACT and 5' TTACCAGCACAGGATCAAATGG with 5' CGGAAGTAGAATCTCACAGCAC, respectively. Relative gene expression was determined using qBase plus using *Ppia* and *Rpl* reference genes (Biogazelle, Zwijnaarde, Belgium).

## Imaging

For scanning electron microscopy, tissue was fixed in 2% *p*-formaldehyde and 2.5% glutaraldehyde, followed by 1% osmium tetroxide and dehydration via ethanol prior to drying in hexamethyldisilazane. After mounting and sputter coating (Auto SC; Agar) with platinum, tissue was examined in a JEOL 7401F (JEOL, Tokyo, Japan) scanning electron microscope.

For macroscopic imaging of the thymus surface, the dissected thymus was incubated with topically applied crystal violet dye for 1 min, washed with PBS/BSA, and photographed with a Leica DFC295 (Leica, Wetzlar, Germany) digital camera. For immunofluorescence, thymic sections were OCT-embedded and stained as previously described [42]. The following reagents were used for staining: 4',6-diamidino-2-phenylindole (DAPI, Invitrogen), rabbit anti-Keratin 5 (PRB-160P; Covance, Berkeley, CA, USA), rat anti-Keratin 8 supernatant (Troma-1; DSHB, Iowa City, IA, USA), rabbit anti-Keratin 14 (PRB-115P-100, Covance), rabbit anti-Keratin 10 (PRB-159P, Covance), rat anti-MECA-32 supernatant (MECA-32, ATCC), rabbit anti-Claudin 3 (Invitrogen), rabbit anti-Claudin-4 (Invitrogen), rat anti-VAP1 (Hycult Biotech, Plymouth Meeting, PA, USA), goat anti-Aire (D-17, Santa Cruz Biotechnology, Dallas, TX, USA), rat anti-CD4 (GK1.5, A. Farr), rabbit anti-Desmin (Thermo Fisher Scientific, Rockford, IL, USA), rat anti-ERTR7 (A. Farr), Rat-Epcam (G8.8; A. Farr), rat anti-F4/80 (A. Farr), Ulex Europaeus Agglutinin biotin (Vector labs, Burlingame, CA, USA), rabbit anti-p63 (poly6190, Biolegend), rat anti-CD19 (1D3, A. Farr), hamster anti-CD11c biotin (N418,

eBioscience), rat anti-CD4 biotin (RM4-5, eBioscience), rat anti-CD8a allophycocyanin (53-6.7, eBioscience), donkey anti-rabbit Alexa-488 (A21206, Thermo Fisher Scientific), donkey anti-Goat Alexa-546 (A11056, Thermo Fisher Scientific), goat anti-rat Alexa-555 (A21434, Thermo Fisher Scientific), chicken anti-rat Alexa-546 (A21482, Thermo Fisher Scientific), streptavidin Alexa-546 (S11225, Thermo Fisher Scientific), and streptavidin Alexa-546 (S32357, Thermo Fisher Scientific). All images were acquired using a Zeiss LSM 510 meta-confocal (Zeiss, Oberkochen, Germany) microscope.

For immunohistochemistry, thymic sections were acetone-fixed and blocked with PBS, 2% BSA, 10% goat serum prior to two-stage staining. Sections were stained with rabbit anti-Keratin 14 (PRB-115P-100, Covance) and goat anti-Rabbit (H + L) HRP (Thermo Fisher Scientific) before developing with 3,3'-diaminobenzidine, followed by staining with rat anti-MECA-32 (MECA-32, ATCC) and goat anti-Rat (H + L) HRP before developing with 3-amino-9-ethylcarbazole (Sigma-Aldrich, St. Louis, MO, USA). Images were acquired using a Leica M125 microscope equipped with a DFC295 digital camera. For 3D reconstruction, serial images were modeled using BioVis3D 3.1 software (BioVis3D, Montevideo, Uruguay).

## Genome-wide linkage analysis and statistical analysis

(C57BL/6 x FVB/N).F2 intercross mice were assessed at 4 weeks of age for thymic structural abnormalities by immunofluorescence. Genomic DNA was prepared using the DNeasy Blood and Tissue Kit (Qiagen) and SNP typing was performed on the Illumina Golden Gate platform at the “Mutation Mapping and Developmental Analysis Project” (MMDAP; Brigham and Women’s Hospital, Harvard Medical School). Noninformative SNPs were manually filtered and the relative location of informative SNPs was confirmed by recombination frequency in the cohort. Standard interval mapping was performed using R/qtl software package (version 1.23-16). LOD scores were calculated as a measurement for linkage at each marker, using both standard interval mapping and extended Haley–Knott regression. Statistical significance of the results was evaluated by testing 1000 permutation replicates. For experiments other than genetic linkage, statistical analysis was performed using Prism (Graphpad, La Jolla, CA, USA). A significance threshold of 5% in a Student’s *t*-test was maintained throughout the study.

**Acknowledgments:** We thank Andrew Farr for insightful advice and kindly providing us with hybridomas. We would also like to thank S. Schoenfeldt and J. Houghton for mouse colony support. This study was supported by the FWO and VIB. S.M.S is an FWO postdoctoral fellow.

**Conflict of interest:** The authors declare no financial or commercial conflict of interest.

## References

- 1 Miller, J. F., The golden anniversary of the thymus. *Nat. Rev. Immunol.* 2011. **11**: 489–495.
- 2 Miller, J. F., Immunological function of the thymus. *Lancet* 1961. **2**: 748–749.
- 3 Prockop, S. E. and Petrie, H. T., Regulation of thymus size by competition for stromal niches among early T cell progenitors. *J. Immunol.* 2004. **173**: 1604–1611.
- 4 Goldschneider, I., Cyclical mobilization and gated importation of thymocyte progenitors in the adult mouse: evidence for a thymus-bone marrow feedback loop. *Immunol. Rev.* 2006. **209**: 58–75.
- 5 Schnell, F. J., Zoller, A. L., Patel, S. R., Williams, I. R. and Kersh, G. J., Early growth response gene 1 provides negative feedback to inhibit entry of progenitor cells into the thymus. *J. Immunol.* 2006. **176**: 4740–4747.
- 6 Foss, D. L., Donskoy, E. and Goldschneider, I., The importation of hematogenous precursors by the thymus is a gated phenomenon in normal adult mice. *J. Exp. Med.* 2001. **193**: 365–374.
- 7 Martins, V. C., Ruggiero, E., Schlenner, S. M., Madan, V., Schmidt, M., Fink, P. J., vonKalle, C. et al., Thymus-autonomous T cell development in the absence of progenitor import. *J. Exp. Med.* 2012. **209**: 1409–1417.
- 8 Gossens, K., Naus, S., Corbel, S. Y., Lin, S., Rossi, F. M., Kast, J. and Ziltener, H. J., Thymic progenitor homing and lymphocyte homeostasis are linked via S1P-controlled expression of thymic P-selectin/CCL25. *J. Exp. Med.* 2009. **206**: 761–778.
- 9 Anderson, G., Harman, B. C., Hare, K. J. and Jenkinson, E. J., Microenvironmental regulation of T cell development in the thymus. *Semin. Immunol.* 2000. **12**: 457–464.
- 10 Gray, D. H., Seach, N., Ueno, T., Milton, M. K., Liston, A., Lew, A. M., Goodnow, C. C. et al., Developmental kinetics, turnover, and stimulatory capacity of thymic epithelial cells. *Blood* 2006. **108**: 3777–3785.
- 11 Dooley, J. and Liston, A., Molecular control over thymic involution: from cytokines and microRNA to aging and adipose tissue. *Eur. J. Immunol.* 2012. **42**: 1073–1079.
- 12 Shanley, D. P., Aw, D., Manley, N. R. and Palmer, D. B., An evolutionary perspective on the mechanisms of immunosenescence. *Trends Immunol.* 2009. **30**: 374–381.
- 13 Chidgey, A. P., Seach, N., Dudakov, J., Hammett, M. V. and Boyd, R. L., Strategies for reconstituting and boosting T cell-based immunity following haematopoietic stem cell transplantation: pre-clinical and clinical approaches. *Semin. Immunopathol.* 2008. **30**: 457–477.
- 14 Nikolich-Zugich, J., Ageing and life-long maintenance of T-cell subsets in the face of latent persistent infections. *Nat. Rev. Immunol.* 2008. **8**: 512–522.
- 15 Eaton, S. M., Burns, E. M., Kusser, K., Randall, T. D. and Haynes, L., Age-related defects in CD4 T cell cognate helper function lead to reductions in humoral responses. *J. Exp. Med.* 2004. **200**: 1613–1622.
- 16 Yang, X., Stedra, J. and Cerny, J., Relative contribution of T and B cells to hypermutation and selection of the antibody repertoire in germinal centers of aged mice. *J. Exp. Med.* 1996. **183**: 959–970.
- 17 Dorshkind, K., Montecino-Rodriguez, E. and Signer, R. A., The ageing immune system: is it ever too old to become young again? *Nat. Rev. Immunol.* 2009. **9**: 57–62.
- 18 Chidgey, A., Dudakov, J., Seach, N. and Boyd, R., Impact of niche aging on thymic regeneration and immune reconstitution. *Semin. Immunol.* 2007. **19**: 331–340.
- 19 Taub, D. D. and Longo, D. L., Insights into thymic aging and regeneration. *Immunol. Rev.* 2005. **205**: 72–93.
- 20 Zhu, X., Gui, J., Dohkan, J., Cheng, L., Barnes, P. F. and Su, D. M., Lymphohematopoietic progenitors do not have a synchronized defect with age-related thymic involution. *Aging Cell* 2007. **6**: 663–672.
- 21 Aw, D., Silva, A. B., Maddick, M., von Zglinicki, T. and Palmer, D. B., Architectural changes in the thymus of aging mice. *Aging Cell* 2008. **7**: 158–167.
- 22 Sun, L., Guo, J., Brown, R., Amagai, T., Zhao, Y. and Su, D. M., Declining expression of a single epithelial cell-autonomous gene accelerates age-related thymic involution. *Aging Cell* 2010. **9**: 347–357.
- 23 Chen, L., Xiao, S. and Manley, N. R., Foxn1 is required to maintain the postnatal thymic microenvironment in a dosage-sensitive manner. *Blood* 2009. **113**: 567–574.
- 24 Min, D., Panoskaltis-Mortari, A., Kuro, O. M., Hollander, G. A., Blazar, B. R. and Weinberg, K. I., Sustained thymopoiesis and improvement in functional immunity induced by exogenous KGF administration in murine models of aging. *Blood* 2007. **109**: 2529–2537.
- 25 Nabarra, B., Mulotte, M., Casanova, M., Godard, C. and London, J., Ultrastructural study of the FVB/N mouse thymus: presence of an immature epithelial cell in the medulla and premature involution. *Dev. Comp. Immunol.* 2001. **25**: 231–243.
- 26 Papadopoulou, A. S., Dooley, J., Linterman, M. A., Pierson, W., Ucar, O., Kyewski, B., Zuklys, S. et al., The thymic epithelial microRNA network elevates the threshold for infection-associated thymic involution via miR-29a mediated suppression of the IFN-alpha receptor. *Nat. Immunol.* 2012. **13**: 181–187.
- 27 Kyewski, B. A., Seeding of thymic microenvironments defined by distinct thymocyte-stromal cell interactions is developmentally controlled. *J. Exp. Med.* 1987. **166**: 520–538.
- 28 Lind, E. F., Prockop, S. E., Porritt, H. E. and Petrie, H. T., Mapping precursor movement through the postnatal thymus reveals specific microenvironments supporting defined stages of early lymphoid development. *J. Exp. Med.* 2001. **194**: 127–134.
- 29 Min, H., Montecino-Rodriguez, E. and Dorshkind, K., Reduction in the developmental potential of intrathymic T cell progenitors with age. *J. Immunol.* 2004. **173**: 245–250.
- 30 Tzeng, T. C., Chyou, S., Tian, S., Webster, B., Carpenter, A. C., Guaiquil, V. H. and Lu, T. T., CD11c(hi) dendritic cells regulate the re-establishment of vascular quiescence and stabilization after immune stimulation of lymph nodes. *J. Immunol.* 2010. **184**: 4247–4257.
- 31 Li, L., Hsu, H. C., Grizzle, W. E., Stockard, C. R., Ho, K. J., Lott, P., Yang, P. A. et al., Cellular mechanism of thymic involution. *Scand. J. Immunol.* 2003. **57**: 410–422.
- 32 Sutherland, J. S., Goldberg, G. L., Hammett, M. V., Uldrich, A. P., Berzins, S. P., Heng, T. S., Blazar, B. R. et al., Activation of thymic regeneration in mice and humans following androgen blockade. *J. Immunol.* 2005. **175**: 2741–2753.
- 33 Yang, H., Youm, Y. H. and Dixit, V. D., Inhibition of thymic adipogenesis by caloric restriction is coupled with reduction in age-related thymic involution. *J. Immunol.* 2009. **183**: 3040–3052.
- 34 Ruiz, P., Dunon, D., Hesse, B. and Imhof, B. A., T lymphocyte pre-cursors adhere to thymic endothelium. In Imhof, B. A., Berrih-Aknin, S. and Ezine, S. (Eds.), *Lymphatic tissues and in vivo immune responses*, M. Dekker, New York, 1991, pp. 963.
- 35 Lewis, J. M., Girardi, M., Roberts, S. J., Barbee, S. D., Hayday, A. C. and Tigelaar, R. E., Selection of the cutaneous intraepithelial gammadelta<sup>+</sup> T cell repertoire by a thymic stromal determinant. *Nat. Immunol.* 2006. **7**: 843–850.
- 36 Turchinovich, G. and Hayday, A. C., Skint-1 identifies a common molecular mechanism for the development of interferon-gamma-secreting

- versus interleukin-17-secreting gammadelta T cells. *Immunity* 2011. **35**: 59–68.
- 37 Pang, W. W., Price, E. A., Sahoo, D., Beerman, I., Maloney, W. J., Rossi, D. J., Schrier, S. L. et al., Human bone marrow hematopoietic stem cells are increased in frequency and myeloid-biased with age. *Proc. Natl. Acad. Sci. USA* 2011. **108**: 20012–20017.
- 38 Dudakov, J. A., Khong, D. M., Boyd, R. L. and Chidgey, A. P., Feeding the fire: the role of defective bone marrow function in exacerbating thymic involution. *Trends Immunol.* 2010. **31**: 191–198.
- 39 Zhang, S. L. and Bhandoola, A., Trafficking to the thymus. *Curr. Top Microbiol. Immunol.* 2014. **373**: 87–111.
- 40 Jenkinson, W. E., Rossi, S. W., Parnell, S. M., Jenkinson, E. J. and Anderson, G., PDGFRalpha-expressing mesenchyme regulates thymus growth and the availability of intrathymic niches. *Blood* 2007. **109**: 954–960.
- 41 Taketo, M., Schroeder, A. C., Mobraaten, L. E., Gunning, K. B., Hanten, G., Fox, R. R., Roderick, T. H. et al., FVB/N: an inbred mouse strain preferable for transgenic analyses. *Proc. Natl. Acad. Sci. USA* 1991. **88**: 2065–2069.
- 42 Dooley, J., Erickson, M. and Farr, A. G., Alterations of the medullary epithelial compartment in the Aire-deficient thymus: implications for programs of thymic epithelial differentiation. *J. Immunol.* 2008. **181**: 5225–5232.

*Full correspondence:* Dr. Adrian Liston, Department of Microbiology and Immunology, University of Leuven, Leuven 3000, Belgium  
e-mail: [adrian.liston@vib.be](mailto:adrian.liston@vib.be)  
*Additional correspondence:* James Dooley, VIB, University of Leuven, Leuven 3000, Belgium  
Fax: +32-0-163 30591  
e-mail: [dooley@vib-kuleuven.be](mailto:dooley@vib-kuleuven.be)

Received: 21/10/2014  
Revised: 22/12/2014  
Accepted: 23/1/2015  
Accepted article online: 27/1/2015